15th Canadian Masonry Symposium
Ottawa, Canada
June 2-5, 2025

Model Updating of a Masonry Arch Bridge: Evaluating the Effectiveness of Structural Intervention

Andrea Gennaro[i], Matteo Salvalaggio[ii], Filippo Lorenzoni[iii], Luca Tosolini[iv] and Francesca da Porto[v]

ABSTRACT

The seismic performance of masonry arch bridges is of paramount importance, given their historical significance and structural vulnerability to seismic events. A comprehensive understanding of the dynamic behavior of these structures is essential to ensure structural safety and to evaluate possible effective intervention strategies. In addition, evaluating the effectiveness of the executed interventions is also crucial to confirm that the implemented measures provide the expected improvements.

This study assesses the efficacy of a structural intervention on a masonry arch bridge through the application of model updating techniques based on post-intervention data. The bridge was restored in order to improve its resistance to seismic events. After the restoration work, Ambient Vibration Tests (AVTs) were conducted in order to capture the bridge's modal characteristics, including natural frequencies and mode shapes. The model updating process involved calibrating the Finite Element (FE) model to align with the measured dynamic responses, adjusting parameters such as material properties, boundary conditions, and structural details. Despite the absence of pre-intervention dynamic data, the updated FE model provides an accurate representation of the bridge's current state, allowing for an indirect assessment of the intervention's effectiveness in enhancing seismic performance.

KEYWORDS

Masonry arch bridge, Finite Element Modelling, Experimental test, Model updating, Ambient Vibration Tests

[i] Research Fellow, University of Padua, Padua, Italy, andrea.gennaro@unipd.it
[ii] Postdoctoral Researcher, University of Minho, Minho, Portugal, matteo.salvalaggio@civil.uminho.pt
[iii] Research Associate, University of Padua, Padua, Italy, filippo.lorenzoni@unipd.it
[iv] PhD Student, University of Padua, Padua, Italy, francesca.daporto@unipd.it
[v] Full Professor, University of Padua, Padua, Italy, francesca.daporto@unipd.it

INTRODUCTION

Over the past decades, the Finite Element (FE) method has been extensively adopted across various engineering disciplines proving indispensable for simulating complex structural behaviors. The utility of the method extends to a wide range of model-based activities, including damage identification, structural health monitoring (SHM), reliability and safety assessments, as well as risk analyses [1]. Nevertheless, the capacity of an FE model to accurately represent the actual structure—a "high-fidelity" model—is contingent upon its precise replication of the underlying physical and mechanical properties [2]. In practice, discrepancies frequently emerge between numerical predictions and observed responses, largely due to uncertainties in material characteristics, geometric configurations, boundary conditions, and other parameters not fully captured in the original design assumptions [3]. To address these gaps, experimental measurements are crucial. Dynamic identification tests, particularly Ambient Vibration Tests (AVTs), are effective tools for characterizing a structure's dynamic properties—such as natural frequencies and mode shapes—under ambient conditions [4–8]. By integrating the insights gleaned from AVTs, FE models can be rigorously validated and refined. This iterative process, known as Finite Element Model Updating (FEMU), involves the systematic adjustment of uncertain parameters until the numerical results align closely with the measured response [9]. The FEMU method has been demonstrated to be particularly beneficial not only for routine validation but also for the assessment of the impact of strengthening or rehabilitation interventions [10]. In the aftermath of a reinforcement procedure, it is essential to ascertain whether the intended improvements—enhanced stiffness, reduced vulnerabilities, and improved overall resistance—have indeed been realized. By comparing the dynamic characteristics of a structure before and after an intervention, FEMU enables: (i) evaluation of the intervention's efficacy against expected performance gains; (ii) long-term monitoring of the reinforced structure's behavior to detect emerging deficiencies; and (iii) improved guidance for future interventions. Of particular relevance within this context are masonry arch bridges (MABs), which represent a significant portion of both historical and modern transportation networks. Due to their inherent structural complexity MABs have been the subject of extensive investigation in the framework of FE analysis and model updating supported by dynamic identification tests [11–14]. In this context, the present study focuses on a masonry arch bridge that has underwent a structural intervention aimed at increasing its seismic resistance. Following the restoration, AVTs were carried out to capture the bridge's current modal characteristics. Although pre-intervention dynamic data were unavailable, the application of FEMU techniques to the post-intervention data facilitated the calibration of a corresponding FE model. By aligning the model's predictions with the measured dynamic properties, it is possible to indirectly evaluate the effectiveness of the intervention in enhancing the structural performance of the bridge. This research thus illustrates how FEMU based on AVTs can be a powerful tool in validating and quantifying the real-world benefits of rehabilitation strategies.

MATERIAL AND METHODS

Description of the case study

The Gresal Bridge (Fig. 1), constructed in the early 19th century in northeastern Italy, is a three-span stone masonry arch bridge measuring 67.40 m in total length, with each span approximately 15 m. It's nearly semicircular arches, featuring a radius of about 7.39 m, rest on two piers that reach up to 12.75 m in height. The roadway width is 6.09 m, and the spandrel walls extend above the deck to form two parapets. Originally built for vehicular traffic, the structure is of regional significance and provides an important crossing over the Gresal River. To improve the bridge's seismic resistance, a multi-stage strengthening intervention was implemented. First, a portion of the internal infill was carefully removed, retaining only the material with the most favorable mechanical properties to keep the vault under compression. Subsequently, a 25 cm-thick reinforced concrete (RC) slab was cast over the full length of the deck and anchored to the abutments. To further stabilize the structure, micro-piles were introduced at the abutments to efficiently transfer loads and counteract overturning. Next, high-strength vertical bars (26.5 mm in diameter) were installed through the full height of the piers, creating a direct connection between the RC slab and the foundations (Fig. 2). This measure enhanced the bridge's load-bearing capacity in both the longitudinal and transverse directions. Finally, the spandrel walls were restored using traditional techniques, which involved cleaning, replacing damaged bricks, repointing with a suitable hydraulic lime-based mortar, and inserting stainless steel bars into the mortar joints. The effectiveness of the strengthening technique was evaluated using nonlinear numerical models, which compared the seismic capacity of the bridge before and after the retrofit. The retrofit increased the bridge capacity—in terms of ultimate displacement in the inelastic field—in both the longitudinal and transverse directions [15].

Figure 1: Panoramic view and piers of the Gresal Bridge, IT

a) b)

Figure 2: a) high strength bars placed inside the two central slender piers and b) micro-piles disposed in two inclined rows outside the existing masonry abutments

Structural investigation

Before the implementation of the retrofit intervention, a comprehensive structural investigation was conducted. This involved the extraction of three core samples and the execution of a detailed geometric survey. Two vertical cores were extracted from the arch's central area and a pier, while a third was drilled from the abutment along an inclined plane. These samples enabled the determination of the masonry thickness, the composition of the material layers between the pavement and the arch barrel, and the mechanical properties of the infill. At the midpoint of the arch, the infill layer is approximately 0.75 meters in thickness, with a masonry thickness of approximately 0.60 meters. The infill is primarily composed of loose stones and pebbles.

Ambient Vibration Test

The AVT was conducted after the structural strengthening intervention using eight high-sensitivity piezoelectric accelerometers capable of detecting vibrations up to 100 Hz. Three accelerometers were positioned at midspan to serve as reference points, while an additional five were simultaneously placed in various locations. Subsequently, the five devices were relocated through three consecutive data acquisition sessions to ensure comprehensive coverage of the structure as reported in Fig. 3 (three different setups). The sensors, offering a resolution of 6 µg, were connected via coaxial cables to a computer equipped with a data acquisition system. Ambient vibrations were recorded for approximately 11 minutes at a sampling frequency of 100 Hz, without interruption to vehicular traffic. The time histories were processed using pLSCF [16–18] method. The considerable stiffness and mass of the bridge presented a significant challenge in the extraction of its modal parameters from ambient vibrations.

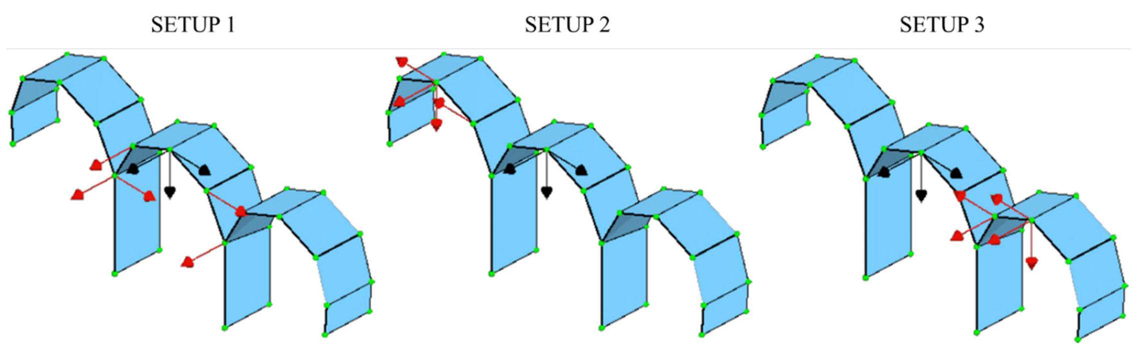

Figure 3: Setups of sensors

Numerical model

The 3D model of the Gresal bridge (Fig. 4) was developed using DIANA FEA software [19]. The structure was represented utilizing 8-node tetrahedral elements with a mesh size of 0.5 m for both the fill material and the masonry. The profile of the haunch filling was hypothesized based on literature studies and the surveys conducted. Transverse micro-piles on the abutments and vertical bars on the piers were modeled as "*Embedded Reinforcement*" elements constrained at their bases, while in the longitudinal direction, the presence of micro-piles was simulated by constraining displacements at the slab level. The reinforced concrete slab was modeled using 8-node tetrahedral elements with material properties corresponding to C30/37 concrete. To better simulate the real behavior of the bridge abutments, the restraint provided by the soil behind the abutments was modeled using a series of translational springs. The translational stiffness of these springs was determined based on the geotechnical characteristics of the soil, described as compact clay transitioning into gravelly clay at greater depths, with a rock substratum beneath gravelly soils. According to classical geotechnical models, the lateral subgrade reaction modulus for compact clay typically ranges between 5000 and 15000 kN/m², depending on the degree of compaction and the soil's shear strength [20,21]. For the specific conditions of this site, a medium value of 10000 kN/m² was adopted, considering the soil's composition and depth. The translational stiffness per spring was calculated by multiplying the subgrade reaction modulus by the influence length of each node, which in this case was 0.5 m. The resulting stiffness value per unit length was then converted to 5000 N/mm. Regarding the mechanical properties of the materials, based on the results from the surveys conducted, reference values were assumed for the bridge masonry structure corresponding to natural stone resistant elements, particularly of the "compact limestone" type [22].

- Mass Density ρ [T/m³] = 2.4÷2.7.
- Compressive strength f_{bm} [MPa] = 50÷150.
- Young's modulus E [GPa] = 20.0-80.0.

Observations indicated that the mortar joints in the masonry walls exhibit good characteristics. It was assumed that the actual characteristics of the mortar are intermediate between a class M10 and a class M15 mortar [22]:

Table 1: Comparison between M10 and M15 mortar properties

Compressive strength	**Class M10**	**Class M15**
Mortar average compressive strength f_m [MPa]	10.0	15.0
Masonry block characteristic compressive strength $f_{bk} = 0.75 f_{bm}$ [MPa]	> 40	> 40
Element characteristic compressive strength f_k [MPa]	12.0	14.3

By averaging the characteristic compressive strengths of the masonry, the result is f_k=13.15 MPa. In the absence of direct experimental tests, the following calculation values can be assumed with regard to the elastic characteristics of the masonry [22]:

(1) $E = 1000 f_k$

Based on the previously calculated compressive strength, and assuming an intermediate behavior between class M10 and class M15 for the mortar, the Young's modulus E of the masonry falls within the range of values between a minimum of 12.0 GPa and a maximum of 14.3 GPa, with an average value of 13.15 GPa. This justifies the use of a Young's modulus of 12.0 GPa in the numerical model, with a Poisson's ratio of 0.2. Regarding the fill material, the core samples revealed that it consists of loose, coarse, incoherent material containing stones, pebbles, fragments of stone blocks, and well-compacted solid bricks. According to literature and regulations, historic masonry bridges with similar compositions typically exhibit a Young's modulus ranging from 1.0 GPa to 3.0 GPa [23]. Given the lower mechanical properties of the fill material compared to the external stone masonry, this supports the decision to adopt a lower Young's modulus of 1.0 GPa in the numerical model. For the fill material, Poisson's ratio of 0.15 was adopted. Non-structural masses, including the weight of the road pavement were included in the model. An eigenvalue analysis was performed, and the first three mode shapes are illustrated in Fig. 5.

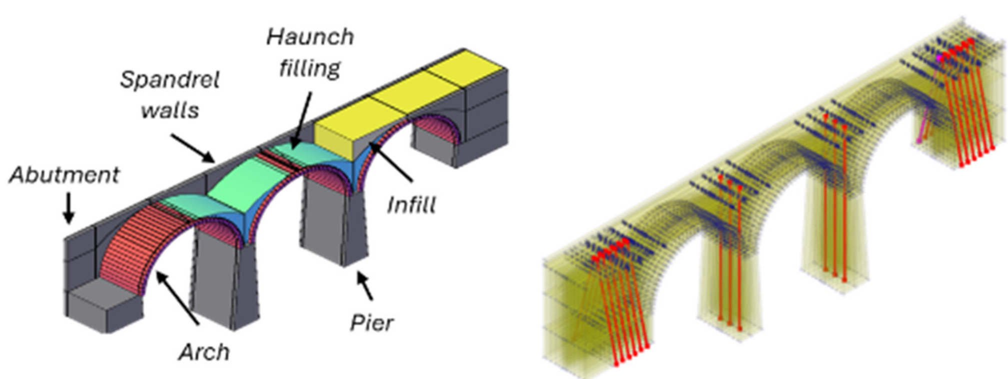

Figure 4: 3D FE model of the Gresal Bridge

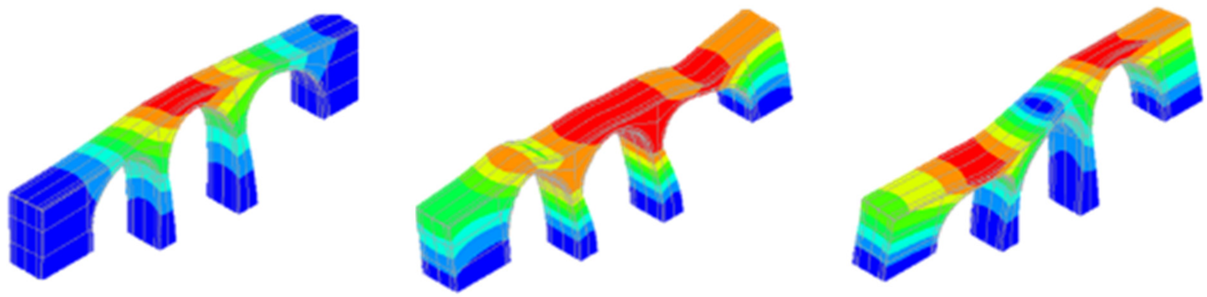

a) b) c)

Figure 5: 3D graphical representation of the numerical modal shapes for the first three modes identified: a) 1st Mode — f = 4.493Hz; b) 2nd Mode — f = 7.168Hz; c) 3rd Mode — f = 7.278Hz

Model updating

The FEMU was conducted with the use of FEMtools 3.6 [24] software, employing a Bayesian Parameter Estimation (BPE) approach. The BPE method is an iterative procedure based on a sensitivity matrix, which is calculated as follows:

$$(2)\ \{R_e\} = \{R_a\} + [S](\{P_u\} - \{P_0\})$$

where $\{R_e\}$ is the vector containing the reference system responses (experimental data); $\{R_u\}$ is the vector containing the predicted system responses for a given state $\{P_0\}$ of the parameters values; $\{P_u\}$ is the vector containing the updated parameter values, and $[S]$ is the sensitivity matrix. The discrepancy between the initial model predictions and the test data is resolved by the minimization of a weighted error, ε, which is given by:

$$(3)\ \varepsilon = \Delta R^T C_R \Delta R + \Delta P^T C_P \Delta P$$

where, C_R represents the weighting matrix for the experimental data (eigenfrequencies), whereas C_P corresponds to the weighting matrix for the updated model parameters. The weighting matrixes are calculated as follows:

$$(4)\ C_{R_i} = \left(\frac{1}{R_i}\right)^2 \cdot \left(\frac{1}{c_{r_i}}\right)^2 \qquad C_{P_i} = \left(\frac{1}{P_i}\right)^2 \cdot \left(\frac{1}{c_{p_i}}\right)^2$$

where, R_i and P_i represent, respectively, the value of the response and of the parameter i, while c_{r_i} and c_{p_i} respectively indicate the scatter value of the response and of the parameter i. In this case, the values assumed are $c_{r_i} = 0.01$ and $c_{p_i} = 0.25$. The stop criterion assumed is based on the Convergence Criterion (CC), which is defined as follows:

$$(5)\ CC = \frac{1}{n_{modes}} \sum_{i=1}^{n_{modes}} C_{r_i} \frac{|\Delta f_i|}{f_i} \qquad C_r = \sum_{i=1}^{n_{modes}} C_{ri}$$

where, Δf_i denotes the discrepancy between the updated numerical frequency and the experimental frequency f_i, the expected relative error equivalent to $C_{ri} = 100c_{r_i}$. As each iteration was completed, the values of the CC were reassessed. The CC has been set at $CC < 0.1\%$ or a maximum of 50 update iterations.

RESULTS

Summary of AVT results

Fig. 6 illustrates that the first three extracted vibration modes are, respectively, bending in the transverse direction, bending in the longitudinal direction, and torsional. Table 2 presents the comparison between the experimental modal characteristics, estimated using the pLSCF method, and the numerical results from the initial FE model. A significant discrepancy is observed between the experimental frequencies and those predicted by the initial numerical model, as well as in the correlation of the mode shapes, particularly for the first torsional mode. In fact, the maximum frequency error of 37.30% occurs in the first torsional mode, and the Modal Assurance Criterion (MAC) [25] index of 0.660 indicates a weak correlation between the experimental and numerical mode shapes for this mode.

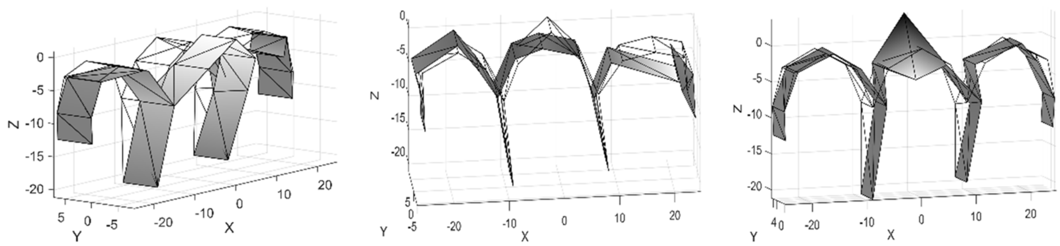

a) b) c)

Figure 6: 3D graphical representation of the experimental modal shapes for the first three modes identified using the pLSFC method: a) 1st Mode — f = 4.930Hz; b) 2nd Mode — f = 8.378Hz; c) 3rd Mode — f = 10.446Hz

Table 2: Comparison between experimental and numerical modal characteristics

Mode	Mode type	pLSCF [Hz]	Initial FEM [Hz]	|Δf| [%]	MAC [-]
1	I° Trans	4.930	4.493	8.864	0.977
2	I° Vert	8.378	6.885	17.820	0.825
3	I° Tors	10.446	6.550	37.297	0.660

Finite Element Model Updating

The process focused on investigating only uncertainties related to the material properties of both the masonry and the infill material. The parameters considered were the Young's modulus, mass density, and Poisson's ratio. Table 3 provides a detailed account of the initial values of the aforementioned parameters, together with the respective variation ranges that were considered in the calibration process. The FE model was updated using the BPE method, with the frequency values of the three modes identified through pLSCF as calibration targets. Owing to the structure’s high stiffness, the mode shapes did not provide sufficient resolution for reliable correlation and were therefore excluded from the calibration process. Table 4 shows the results in terms of frequency and the MAC index for the calibrated model, demonstrating the effectiveness of the calibration process in accurately replicating the dynamic behavior of the bridge. The maximum frequency error decreased from 37.30% to 20.71%, and the MAC indices indicate a good correlation between the experimental and numerical mode shapes. The updated values of the parameters are presented in Table 5. The analysis reveals that the most notable variation occurred in the elastic modulus of the infill material, which exhibited an increase of 200%. This significant increase can be attributed to the intervention phase involving the removal of a thin portion of the internal infill layer. During this process, efforts were made to preserve as much material with the best mechanical properties as possible, as its gravitational load plays a stabilizing role by maintaining the vault voussoirs under compression. The selective removal of weaker infill material and the retention of higher-quality material effectively enhanced the overall mechanical properties of the remaining infill. Consequently, the elastic modulus of the infill material increased substantially, reflecting the improved stiffness due to the preservation of superior material. Conversely, the elastic modulus of the masonry experienced a reduction of 30%, indicating a decrease in stiffness of the masonry. In terms of mass density, masonry presents a increase of 8%, while the infill material's density decreased by 22%. Finally, Poisson's ratio of the masonry was reduced by 25%, while Poisson's ratio for the infill material remained unchanged. A comparison was subsequently performed between the pre- and post-intervention conditions of the bridge. As no dynamic tests were conducted before the seismic retrofitting, it was not possible to calibrate the pre-intervention model. Only the post-intervention model was calibrated. In the absence of detailed experimental data for the pre-intervention state, it was assumed that the post-intervention model could be used as a valid baseline for the pre-intervention condition. Subsequently, all elements related to the seismic retrofitting (micro-piles, vertical bars, and the reinforced concrete slab) were removed from the post-intervention model to represent the pre-intervention state. A comparative analysis of the outcomes of the two models (Fig. 7) allowed an evaluation of the intervention's impact and highlighted the improvement in the bridge's seismic response following the retrofitting.

Table 3: Updating parameters and limit values

n°	Description	Symbol	Ref. Value	Lower limit	Upper limit	Units
1	Masonry elastic modulus	E_m	12.0	8.4	18.0	GPa
2	Infill elastic modulus	E_f	1.0	0.1	3.0	GPa
3	Masonry mass density	ρ_m	2.55	2.4	2.7	t/m^3
4	Infill mass density	ρ_f	1.8	1.4	2.4	t/m^3
5	Masonry Poisson's ratio	ν_m	0.2	0.15	0.3	-
6	Infill Poisson's ratio	ν_f	0.15	0.15	0.2	-

Table 4: Comparison between experimental and numerical modal characteristics of the updated FE

Mode	Mode type	pLSCF [Hz]	Initial FEM [Hz]	Updated FEM [Hz]	MAC [-]
1	I° Trans	4.930	4.493	4.717	0.980
2	I° Vert	8.378	6.885	8.102	0.827
3	I° Tors	10.446	6.550	8.283	0.814
		$\lvert\Delta f_{max}\rvert$	37.30 %	20.71 %	

Table 4: Comparison between the structural properties of the FE model before updating (Ref. value) and after updating (Upd. value)

n°	Description	Symbol	Ref. Value	Upd. value	Δ_{par} [%]	Units
1	Masonry elastic modulus	E_m	12.0	8.4	-30	GPa
2	Infill elastic modulus	E_f	1.0	3.0	+200	GPa
3	Masonry mass density	ρ_m	2.55	2.75	+8	t/m^3
4	Infill mass density	ρ_f	1.8	1.4	-22	t/m^3
5	Masonry Poisson's ratio	ν_m	0.2	0.15	-25	-
6	Infill Poisson's ratio	ν_f	0.15	0.15	0	-

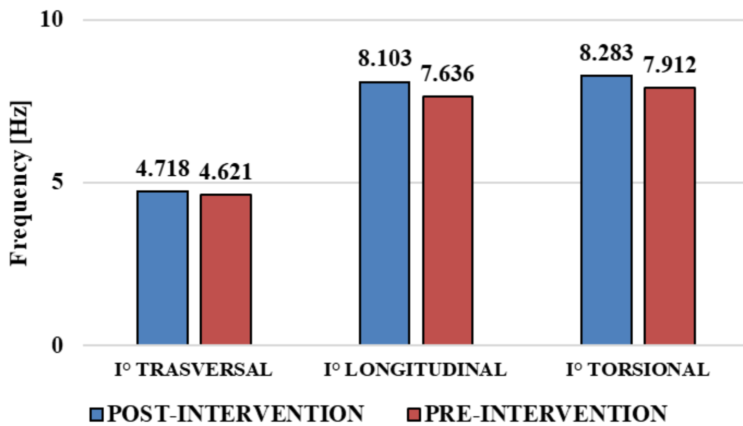

Figure 7: Comparison of natural frequency of pre- and post-intervention FE model

CONCLUSION

This study presented the model updating of a masonry arch bridge, that was subjected to structural intervention, using the results of AVTs conducted after the intervention. The initial FE model, created with DIANA FEA software, exhibited discrepancies in both modal frequencies and MAC indices. In particular, the first torsional mode demonstrated a frequency error of 37.30%, with a MAC index of 0.660. This indicates a poor correlation with the experimental mode shapes. The model updating procedure was performed using the BPE method, in which the material properties of the masonry and the infill were set as variable parameters. This calibration process resulted in a notable reduction in frequency errors, which was reduced to 20.71%. Additionally, the MAC indices exhibited a stronger correlation between the experimental and numerical mode shapes, particularly for the longitudinal and torsional modes.

Finally, a comparison between the pre- and post-intervention conditions was conducted. As no dynamic tests were conducted prior to the seismic retrofitting, it was not possible to directly calibrate the pre-intervention FE model. In order to recreate the pre-intervention FE model, the retrofitting elements were removed from the calibrated post-intervention FE model. This approach allowed for an effective assessment of the structural intervention's efficacy by comparing the two conditions, despite the absence of pre-intervention experimental data.

ACKNOWLEDGEMENTS

Special thanks are also due to ReLUIS, that partially funded this study in the framework of the ReLUIS-DPC Project 2024-2026 – Work Package 5 – Task 4: Retrofit interventions on existing bridges, and of the C.S.LL.PP./ReLUIS Project 2021–2024.

REFERENCES

[1] Brownjohn, J.M.W., Xia, P.Q., Hao, H., and Xia, Y. (2001). "Civil structure condition assessment by FE model updating: Methodology and case studies." *Finite Elements in Analysis and Design*. 37 (10), 761–775.
[2] Mottershead, J.E., Link, M., and Friswell, M.I. (2011). "The sensitivity method in finite element model updating: A tutorial." *Mechanical Systems and Signal Processing*. 25 (7), 2275–2296.
[3] Benedettini, F. and Gentile, C. (2011). "Operational modal testing and FE model tuning of a cable-stayed bridge." *Engineering Structures*. 33 (6), 2063–2073.
[4] Lorenzoni, F., De Conto, N., da Porto, F., & Modena, C. (2019). " Ambient and free-vibration tests to

improve the quantification and estimation of modal parameters in existing bridges." *Journal of Civil Structural Health Monitoring*. 9 (5), 617–637.

[5] Salvalaggio, M., Lorenzoni, F., and Valluzzi, M.R. (2023). "Dynamic Behavior of a Two-Storey Cross Laminated Timber Mockup." *RILEM Bookseries*. 41 137–146.

[6] Salvalaggio, M., Lorenzoni, F., and Valluzzi, M.R. (2024). "Impact of sound-insulated joints in the dynamic behavior of Cross-Laminated Timber structures." *Journal of Building Engineering*. 91 (April), 109525.

[7] Cunha, Á., Caetano, E., Calçada, R., De Roeck, G., and Peeters, B. (2003). "Dynamic measurements on bridges: design, rehabilitation and monitoring." *Proceedings of the Institution of Civil Engineers - Bridge Engineering*. 156 (3), 135–148.

[8] Magalhães, F., Cunha, Á., and Caetano, E. (2008). "Dynamic monitoring of a long span arch bridge." *Engineering Structures*. 30 (11), 3034–3044.

[9] Ewins, D.J. (1986). *Modal Testing: Theory and Practice.* 1st ed. Research Studies Press LTD.

[10] Brownjohn, J.M.W., Moyo, P., Omenzetter, P., and Lu, Y. (2003). "Assessment of Highway Bridge Upgrading by Dynamic Testing and Finite-Element Model Updating." *Journal of Bridge Engineering*. 8 (3), 162–172.

[11] Erduran, E., Gonen, S., Pulatsu, B., and Soyoz, S. (2023). “Damping in masonry arch railway bridges under service loads: An experimental and numerical investigation.” *Engineering Structures*. 294 (April), 116801.

[12] Pantò, B., Ortega, J., Grosman, S., Oliveira, D. V., Lourenço, P.B., Macorini, L., et al. (2024). “Advanced calibration of a 3D masonry arch bridge model using non-destructive testing and numerical optimisation.” *Construction and Building Materials*. 438 (July), 0–2.

[13] Shabani, A. and Kioumarsi, M. (2023). “Seismic assessment and strengthening of a historical masonry bridge considering soil-structure interaction.” *Engineering Structures*. 293 (January), 116589.

[14] Gönen, S. and Soyöz, S. (2021). “Seismic analysis of a masonry arch bridge using multiple methodologies.” *Engineering Structures*. 226 (March 2020).

[15] Tecchio, G., Da Porto, F., Zampieri, P., Modena, C., and Bettio, C. (2012). "Static and seismic retrofit of masonry arch bridges: Case studies." *Bridge Maintenance, Safety, Management, Resilience and Sustainability - Proceedings of the Sixth International Conference on Bridge Maintenance, Safety and Management*. 1094–1098.

[16] Peeters, B., Lowet, G., Van Der Auweraer, H., and Leuridan, J. (2004). "A New Procedure for Modal Parameter Estimation." *Journal of Sound and Vibration*. 24–28.

[17] Peeters, B. and Van Der Auweraer, H. (2005). "PolyMax: a revolution in operational modal analysis."

[18] Peeters, B., Van Der Auweraer, H., Guillaume, P., and Leuridan, J. (2004). "The PolyMAX frequency-domain method: A new standard for modal parameter estimation?" *Shock and Vibration*. 11 (3–4), 395–409.

[19] DIANA FEA BV (2024). *DIANA User’s Manual.*

[20] Terzaghi, K. (1943). *Theoretical soil mechanics.*

[21] Bowles, J.E. (1996). *Foundation Analysis and Design.*

[22] Iacobelli, F. (2008). *Progetto e Verifica delle Costruzioni in Muratura in Zona Sismica.*

[23] Milani, G. and Lourenço, P.B. (2012). "3D non-linear behavior of masonry arch bridges." *Computers and Structures*. 110–111 133–150.

[24] FEMtools (2012). *Model Updating Theoretical Manual.* Leuven, Belgium.

[25] Allemang, R.J. and Brown, D.L. (1982). "A correlation coefficient for modal vector analysis". in: *Proc. Int. Modal Anal. Conf. Exhib.*, pp. 110–116.